Following the Crystallization of Microporous Solids Using EDXRD Techniques

Andrew T. Davies,[†] Gopinathan Sankar,*[,†,‡] C. Richard A. Catlow,*[,†] and Simon M. Clark[‡]

Davy Faraday Research Laboratory The Royal Institution of GB 21 Albemarle Street London W1X 4BS, UK, and CCLRC, Daresbury Laboratory Daresbury Warrington Cheshire WA4 4AD, UK

Received: August 5, 1997; In Final Form: September 6, 1997[⊗]

Energy dispersive X-ray diffraction (EDXRD) techniques are applied to study the development of crystalline phases during the synthesis of microporous materials. We present data for both zeolite A and AlPO-5 systems. We explore the effects of template concentration and of temperature. The measured activation energy for zeolite A of ∼58 kJ mol^{-1} accords well with that observed for other silicate systems. The kinetics revealed by our study accord with the nucleation/growth model of the Avrami−Erofeev treatment.

Introduction

The investigation of the kinetics of nucleation, crystal growth, phase transformation, and dissolution in metastable crystalline systems has long constituted an important area of study within the field of solid-state chemistry. In particular, a detailed understanding of the mechanisms of nucleation and crystal growth of microporous systems has been a major goal of zeolite chemists for many years.[1,2] A better understanding of these processes would allow us to improve our ability to design these industrially important catalytic materials and also to optimize structure-dependent properties such as shape selectivity.[1,3,4] A variety of techniques of varying sophistication, for example ex situ X-ray diffraction,[5,6] NMR,[7] electron microscopy,[8] light scattering,[9−11] and small-angle X-ray and neutron scattering (SAXS and SANS, respectively),[12−15] have been employed to obtain a better understanding of this complex problem. Of these techniques, X-ray diffraction provides a unique opportunity to probe the crystal structure directly and is well suited to in situ studies under operating conditions.[16−21]

Both microporous silicas and aluminophosphates have neutral frameworks, making them unsuitable for catalytic applications. However, substitution by lower-valent heteroatoms produces a charge imbalance in the framework which, if compensated by a proton, produces strong acid catalysts. Examples of such catalysts include aluminosilicates, silicoaluminophosphates (SAPO's), and divalent metal ion substituted aluminophosphates (MeAPOs).[1,6,21−23] In addition, some of the metal ion substituted AlPOs can effectively perform redox catalysis. One such system is Co(II)-substituted AlPO-5.[21]

These materials are generally prepared under hydrothermal conditions, and when information is needed relating to their synthesis, samples may be withdrawn at specific periods in order to follow the progress of their formation. These ex situ methods, although providing useful information, cannot give a complete picture of the processes occurring under reaction conditions. For example, it has been noted that such experiments as well as being susceptible to systematic error can result in intermediate crystal phases being destroyed upon filtration and drying of a sample.[18] There is, therefore, a need for in situ methods in order to understand the mechanisms of hydrothermal reactions under direct synthesis conditions. Recent developments, both in time-resolved diffraction techniques and in situ methods,[16−21] provide a unique opportunity to investigate the formation of microporous solids. Furthermore, this methodology offers a direct measurement of the reaction kinetics and subsequently the activation energy of the process.

Two techniques are available for in situ X-ray diffraction experiments, namely, angle-resolved X-ray diffraction (XRD) and energy-dispersive X-ray diffraction (EDXRD). The former technique uses a less intense monochromatic X-ray beam and thus requires a sample container that does not result in much loss in intensity such as a thin sealed glass or quartz capillary.[20,23] The latter technique instead employs white (polychromatic) radiation from a synchrotron source, covering a wide energy range, that penetrates the stainless steel pressure vessels well suited for hydrothermal synthesis.[16,18,21]

In the present paper we report therefore a time-resolved in situ EDXRD study of the structural changes occurring during the synthesis of two important microporous systems: zeolite A, a nontemplated aluminosilicate system, and a range of heteroatom-substituted members of the AlPO-5 family which require the addition of structure-directing and charge-compensating organic template molecules. Both systems have been the subjects of numerous previous studies of their structural and catalytic properties. This fact, along with their short synthesis times (typically no more than 2 h), makes them well suited for study using in situ synchrotron EDXRD techniques. The present investigation shows clearly the importance of heteroatoms in the growth process and demonstrates the reliability of the EDXRD method in yielding quantitative data on the formation of microporous phases during their synthesis.

Experimental Section

Syntheses. Zeolite A syntheses were carried out using the following gel composition, Al_2O_3:$2SiO_2$:$1.0Na_2O$:$17.5H_2O$, starting materials for this gel being sodium hydroxide pellets (Aldrich), aluminum hydroxide hydrate (Aldrich), and Cab-O-Sil M5 fumed silica (Fluka). In a typical synthesis, the sodium hydroxide was dissolved in distilled water with aluminum hydroxide being subsequently added and the mixture then being thoroughly stirred. To this mixture was added the fumed silica, resulting in the production of a thick, translucent gel. This gel was then placed within a PTFE autoclave liner to a fill volume of 50% and then sealed within the in situ hydrothermal cell. This cell was placed in a preheated furnace in which hydrothermal syntheses were performed at 357, 363, 367, and 378 K for selected time periods.

A range of heteroatom-substituted AlPO-5 compounds were synthesized with the general composition $Me_xAl_{1-x}P_{1-y}Si_yO_4$

* To whom correspondence should be addressed.
† The Royal Institution of GB.
‡ CCLRC, Daresbury Laboratory.
⊗ Abstract published in *Advance ACS Abstracts,* November 1, 1997.

S1089-5647(97)02557-1 CCC: $14.00

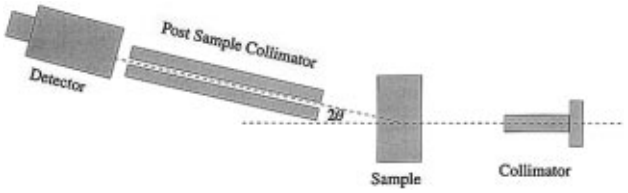

Figure 1. A schematic diagram of the experimental setup used for EDXRD studies at station 16.4 of the Daresbury SRS. The detector is fixed at an angle, 2θ, in such a way that the strong reflections appear within the energy range. The sample in this particular case is a precursor gel contained within a specifically designed autoclave.[16] A 0.5 mm collimator was used in this study.

where Me = Co or Mn, $x = 0$, 0.02, 0.03, 0.04, or 0.06, and $y = 0$ or 0.04. Although a variety of structure-directing and charge-compensating templates are being used in the synthesis of AlPO-5 and its heteroatom variants, in this work we chose to use triethylamine as the templating agent. Starting materials were aluminum hydroxide hydrate (Aldrich), 85 wt % phosphoric acid solution (Aldrich), 99% triethylamine solution (Aldrich), cobalt(II) acetate (Aldrich), manganese(II) acetate (Aldrich), and Cab-O-Sil M5 (Fluka). A typical gel with the composition $0.04MeAc_2{:}0.96Al(OH)_3{:}1.5H_3PO_4{:}0.8NEt_3{:}30H_2O$ (where Me is either Co or Mn) was synthesized as follows. The precursor gel was prepared by first dissolving the cobalt or manganese acetate with the minimum quantity of water, the remainder being added to the phosphoric acid. Subsequently, $Al(OH)_3{\cdot}xH_2O$ was added to this phosphoric acid solution. This mixture was thoroughly stirred before introduction of the cobalt acetate solution. Finally, triethylamine template was added dropwise. A standard 50% fill volume was again used, and hydrothermal synthesis was carried out in a preheated furnace over a temperature range of 436−467 K for an appropriate period.

EDXRD Studies. EDXRD measurements were carried out at station 16.4 of the Daresbury Synchrotron radiation source which operates at 2 GeV, where the typical experimental arrangement used is schematized in Figure 1. The details of the experimental arrangement and the in situ cell design have been published elsewhere.[16] The data were collected under isothermal conditions with zero time (corresponding to the start of data collection) being set to the time when the desired temperature was achieved. The single-element Ge solid-state detector (Canberra) was inclined at a fixed 2θ angle of 1.4556 ± 0.0001°. Typically the time interval between data sets was either 1 or 2 min.

The areas under the reflections of the diffraction pattern were estimated using a suite of programs that allow the use of a range of different peak shape options for curve fitting including both ABFFIT, available as a package in Macintosh format, and PKFIT, a program available at the Daresbury laboratory**.** It should be noted that the recorded data were not corrected for the beam decay, which is typically about 20 mA over a period of 1 h. Our measurements indicated that the region used (normalized intensity range between 0.1 and 0.9) for the evaluation of the activation energy occurs in the time scale of 15 min or less. A closer examination of the data with the inclusion of a beam decay contribution revealed that the small intensity changes are negligible compared to the standard deviation.

Results and Discussion

We now present the results of the characterization during synthesis of the two distinct microporous systems that form the basis of the study: zeolite A, a template-free aluminosilicate system, followed by a range of heteroatom-substituted aluminophosphate materials having the AlPO-5 (AFI) structure. As noted, the synthesis of this second system requires the use of an organic template molecule, in this case triethylamine.

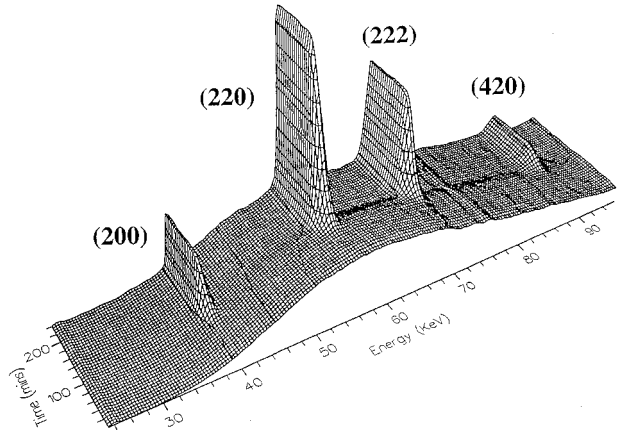

Figure 2. A typical stacked time-resolved EDXRD plot for zeolite A synthesized at 367 K. For clarity, only a limited energy range is displayed. The time zero corresponds to the time at which the temperature of 367 K is achieved and the measurement is started. Measurements were carried out with a time interval of either 1 or 2 min (dead time is of the order of 10^{-6} s and thus ignored) under isothermal conditions.

Zeolite A. Figure 2 shows a typical EDXRD pattern recorded under isothermal conditions during the synthesis of zeolite A at 363 K. After an induction period of ca. 90 min, the reflections associated with the zeolite A structure start to appear. Comparison of the EDXRD pattern of the final product with that of the pattern of a sample prepared in the laboratory confirmed the formation of a pure zeolite A phase. We note in Figure 2 that all the reflections appear simultaneously, suggesting uniform crystal growth. To confirm this observation, each peak was fitted to a curve as shown in Figure 3. The similar behavior of the normalized area under each reflection plotted as a function of time in Figure 4 suggests that uniform growth had taken place along each of the crystallographic directions as would be expected from such a cubic system. It was therefore acceptable to use only the most intense peak in order to carry out the subsequent kinetic studies.

As can be seen in Figure 4, plots of peak area as a function of time were found to produce characteristic sigmoidal curves: an initial period of induction/nucleation during which no peaks were discernible is followed by a period of rapid increase in the area under the peak for a period of ca. 30 min, corresponding to the main phase of crystal growth: a constant value indicating the completion of the crystallization process is then observed. Figure 5 shows the sigmoidal plots for zeolite A, measured at 357, 363, 367, and 378 K which were found to show a clear trend in which increasing the synthesis temperature results in both a reduction in the induction/nucleation period before crystallization begins and an increase in the rate of crystallization. The observed induction period is between 50 and 100 min depending on the synthesis temperature.

The data presented in Figures 4 and 5 can be used to obtain directly the rate constant associated with the crystallization process. As described by others elsewhere,[24,25] we have used the normalized area (α) in the range of values between 0.1 and 0.9 so as to use data only from the main period of crystal growth. The normal procedure involved in estimating the rate constant uses the Avrami−Erofeev equation[24] as described below.

The Avrami−Erofeev approximation gives α (the fraction of crystalline product) according to

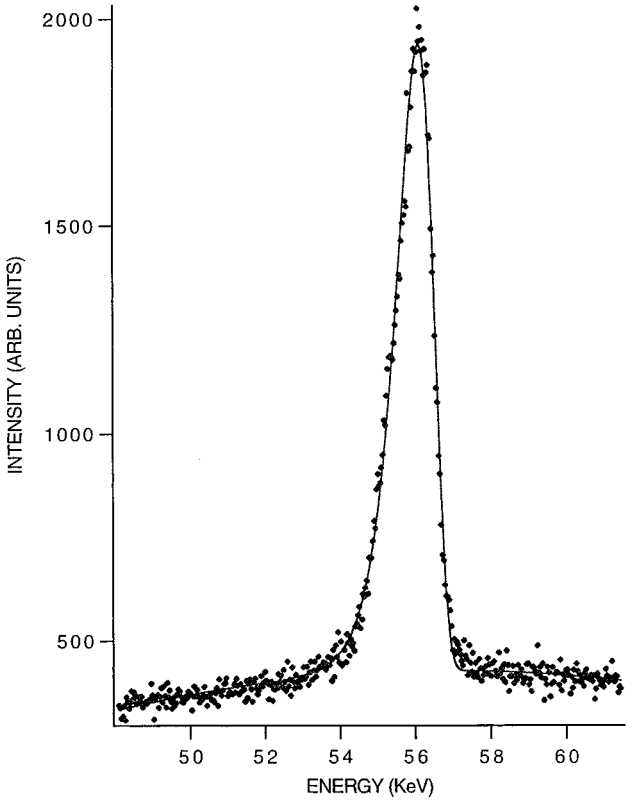

Figure 3. A typical best fit between experimental data (filled diamonds) and calculated profile (solid line) in this case fitting to a Gumbel+ function in order to determine the area under the peak. The strongest reflection, (220), which appears at 56 keV, is used for the kinetic analysis of the formation of the zeolite A phase.

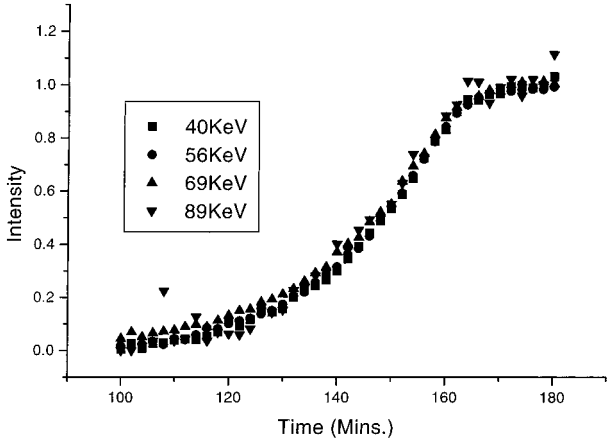

Figure 4. Normalized (against the intensity of the final data point) sigmoidal curves for zeolite A synthesized at 357 K. We have chosen four strong reflections to determine the area under those reflections in order to compare the rate at which the crystalline phase is being formed. Successful superimposition of all the normalized areas under these peaks over the experimental energy range illustrates the uniformity of crystal growth.

$$\alpha = 1 - e^{(-kt)^n}$$

yielding

$$-\ln(1 - \alpha)^{1/n} = kt$$

We therefore plot in Figure 6 the mean value of $-\ln(1 - \alpha)^{1/n}$ vs $(t - t_0)$, where t is the time at which the data were collected after the start of the measurement procedure and t_0 is the induction period which describes the time at which the reflections start to appear.

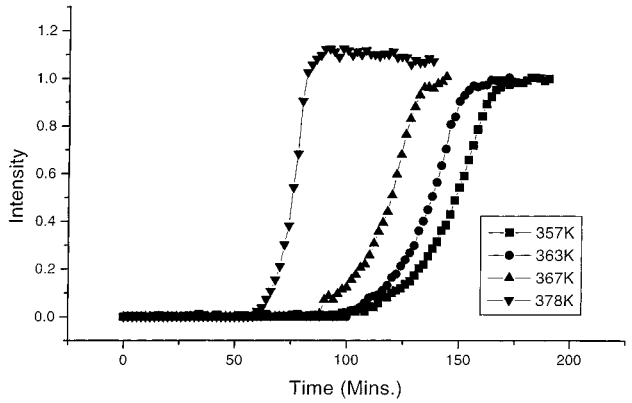

Figure 5. Plots of the normalized area under the reflection (220) appearing at 56 keV (see Figure 2) as a function of time. The different curves represent the measurements carried out at various temperatures under isothermal conditions. (Note that the lines between the points have been added for the sake of clarity and do not represent a mathematical fit.)

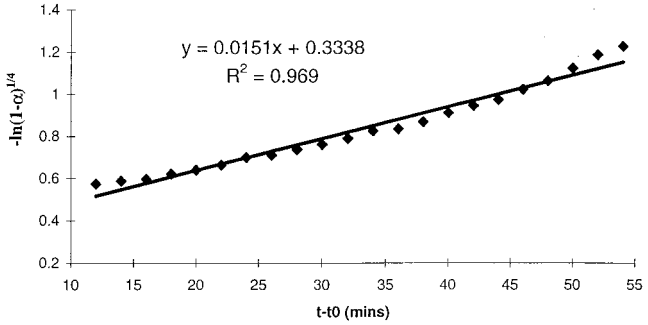

Figure 6. A typical Avrami−Erofeev plot for zeolite A synthesized at 357 K from which the rate constant was evaluated using the time exponent $n = 4$.

The time exponent n indicates the mechanism of nucleation,[24,26] and in cases such as these, typical values used for n are 3 or 4, although larger values have been used.[19] A value of $n = 3$ has been suggested to represent a system with "zero" nucleation, i.e., where all nuclei have formed and no further nucleation takes place. On the other hand, $n = 4$ has been similarly suggested to represent a system undergoing constant nucleation.[24] A value of $n = 4$ was chosen in this case as it is believed that nucleation actually continues to occur for at least the initial period of crystallization.[24,26]

The gradient of the resulting linear fit shown in Figure 6 gives the rate constant k. This rate constant was subsequently calculated for each synthesis temperature. Using the Arrhenius equation, it was then possible to plot $-\ln(k)$ versus reciprocal temperature, T^{-1}, in order to estimate the value of the activation energy of crystallization for the zeolite A synthesis as shown in Figure 7, for which we obtain $E_{A(cryst)} \approx 58$ kJ mol^{-1} (the estimated standard deviation is ca. ± 3 kJ mol^{-1}).

This value is close to those reported in previous studies of the kinetics of hydrothermal silicate synthesis.[27,28] Moreover, it accords well with calculated values of ~60 kJ mol^{-1} calculated by Pereira (1997)[29] for the activation energy for condensation reactions forming Si−O−Si bridges in silicate systems. Differences between our calculated value and those obtained by others[27] can be largely explained by the use of different starting materials, especially silica source materials.

Heteroatom Substituted-Templated Aluminophosphates of the AlPO-5 Family. EDXRD patterns during the synthesis of AlPO-5 and its heteroatom variants were recorded as in the experiments performed for zeolite A. We investigated first the influence of temperature on the formation of the AFI structure

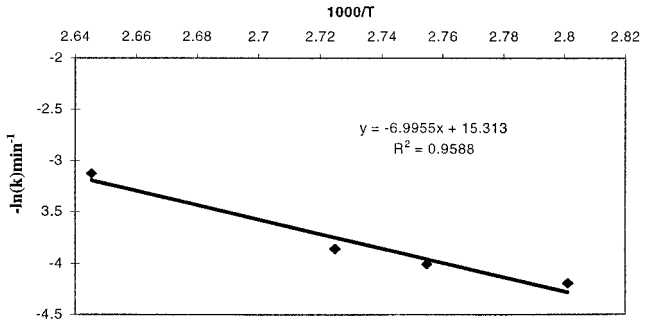

Figure 7. An Arrhenius plot of the rate constant *k* for the synthesis of zeolite A.

from the mother gel for both AlPO-5 and CoAlPO-5 (Co/P = 0.04) and subsequently the effect of the nature of the heteroatom on the formation of the AFI structure at a specific temperature, 436 K.

Figure 8 shows a typical time-resolved EDXRD pattern for AlPO-5 and CoALPO-5 (Co/P = 0.02) recorded at 436 K. One notices that there is slight decrease in the background when the reflections due to the AFI structure start to appear. This may be due to the formation of the crystalline solid which settles in the bottom of the autoclave, thereby increasing the absorption. In the case of AlPO-5 the observed reflections could be readily indexed to the AFI structure with no other phases being observed, whereas for cobalt-substituted AlPO-5, in this case having a Co/P ratio of 0.04, extra peaks were observed, indicating the presence of a second crystalline phase. Upon further investigation, this second phase was confirmed to have a chabazite structure (CHA). This competitive formation of both AFI and CHA phases in the cobalt-containing samples will be addressed later in more detail. Comparison of five reflections available in the energy range under study revealed uniform crystal growth upon normalization of the resulting growth curves. To monitor the formation only of the dominating AFI phase, we considered the most intense reflection which appears at 41 keV and determined the area under this reflection. Plots of the intensity vs synthesis time for both AlPO-5 and CoAlPO-5 (shown in Figure 9, a and b, respectively) synthesized at 436, 449, and 467 K reveal sigmoidal curves with a shortened induction period and an increase in crystallization rate with increasing temperature.

As mentioned previously, we also undertook a detailed study of the effect of different doping levels of Co (Co/P = 0.02, 0.03, 0.04, and 0.06) into the system at a constant temperature of 436 K. One notices clearly the appearance of a new set of reflections for systems containing a Co/P ratio above 0.04, which, as mentioned previously, can readily be indexed to a small pore microporous solid of the structure type CHA (also confirmed by measuring conventional powder diffraction for the Co/P = 0.06 sample). To evaluate the effect of the cobalt concentration on the formation of AFI structure, we plotted the area under the strongest reflection (at 41 keV) vs time in Figure 10, for all the different cobalt concentrations. It is clearly seen that the induction period decreases and the crystallization (AFI structure) rate increases with increasing cobalt content. However, larger loadings of cobalt (Co = 0.06) result in a reversal of this trend, indicating the role of other factors such as the competitive formation of the CHA and AFI structures on the kinetics of crystallization of the AFI structure. This change in the kinetic trend, in particular on the induction period, may be due to the changing distribution of cobalt and template in the system, with the CHA structure preferentially taking up these components, resulting in a reduction in the amounts of cobalt and template available to the AFI. From the trend observed

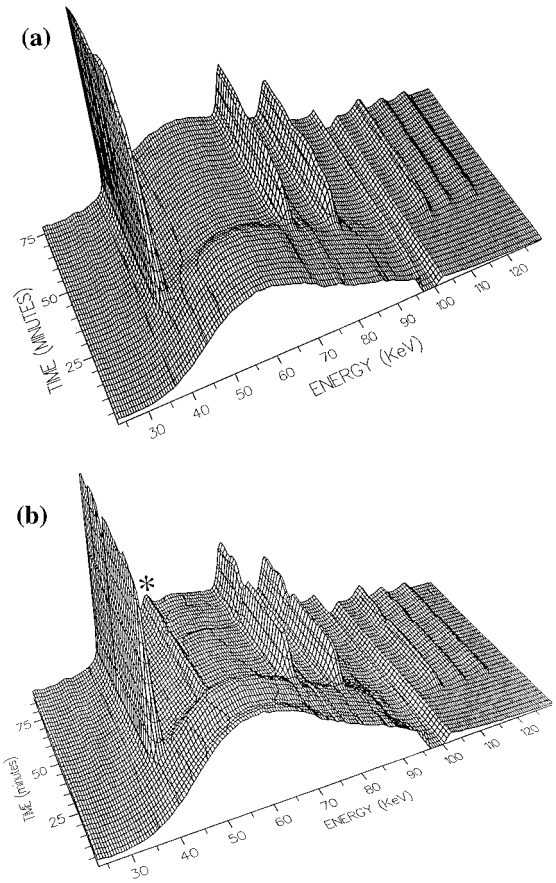

Figure 8. 8. A time-resolved EDXRD stacked plot of (a) $AlPO_4$-5 and (b) $CoAlPO_4$-5 (Co/P = 0.06) recorded at 436 K under isothermal conditions. The simultaneous appearance of a reflection due to the CHA phase (marked by an asterisk) is clear in (b) but is absent in the pure $AlPO_4$-5 synthesis. It should be noted that a further reflection at 98 keV, due to the autoclave, has been excluded from the figure for clarity.

with the lower loadings of Co, this effect would increase the induction period and reduce the rate of synthesis. To elucidate the kinetics and confirm this explanation, high-quality data for the CHA phase are needed. The reason for the formation of both CHA and AFI phases is almost certainly that higher cobalt concentrations require correspondingly larger amounts of triethylamine to charge balance the system, which in turn provides sufficient amounts of organic template molecules for the packing to favor the formation of a competitive chabazite phase, an argument which was supported by our earlier computer modeling studies.[30] This competitive phase was observed above a critical cobalt level of ca. 0.04.[31] It has been noted, by Rey et al.,[21] that the time of disappearance of the metastable chabazite phase is related to the synthesis temperature, with the time from formation to disappearance of the chabazite peaks being much more rapid at higher temperatures (ca. 468 K).

Comparing AlPO-5 with cobalt- and manganese-substituted AlPO-5 (Co/P = 0.04 and Mn/P = 0.04) at a synthesis temperature of 436 K (Figure 11), we note that the induction period reduced and crystallization rate increased for the divalent heteroatom-substituted materials. However, upon comparison of these results with data for SAPO-5 (Si/Al = 0.04) (Figure 10), it was observed that doping with silicon resulted in the opposite effect, with the induction period being extended and the crystallization rate reduced. The result is somewhat surprising, but it may be related to the fact that Mn^{2+} or Co^{2+} exclusively substitute for Al^{3+} whereas Si^{4+} has been noted to substitute for both Al^{3+} and P^{5+}, resulting in island formation.

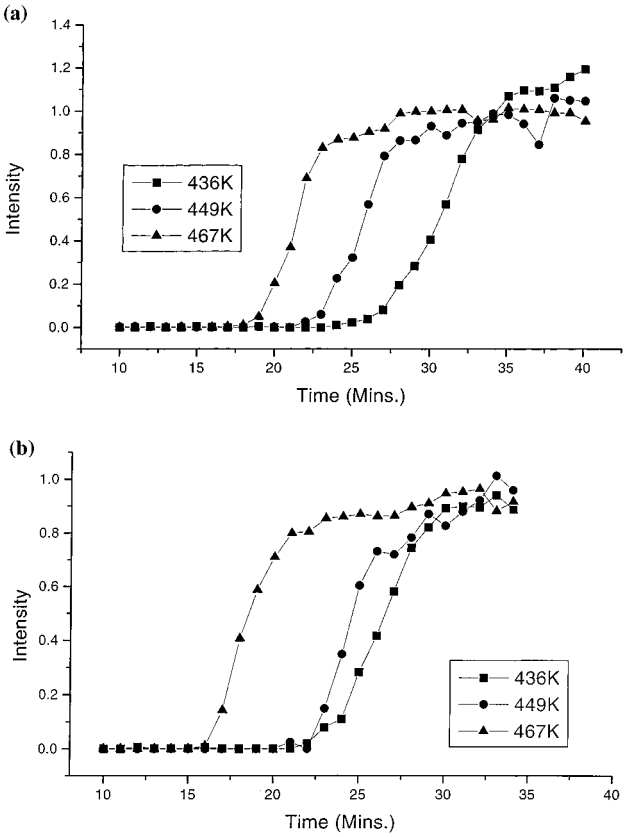

Figure 9. Plots of the normalized area under the reflection which appears at 41 keV (see Figure 8) as a function of time: (a) $AlPO_4$-5 and (b) $CoAlPO_4$-5 (Co/P = 0.04). The different curves represent the measurements carried out at various temperatures under isothermal conditions. (Note that the lines between the points have been added for the sake of clarity and do not represent a mathematical fit.)

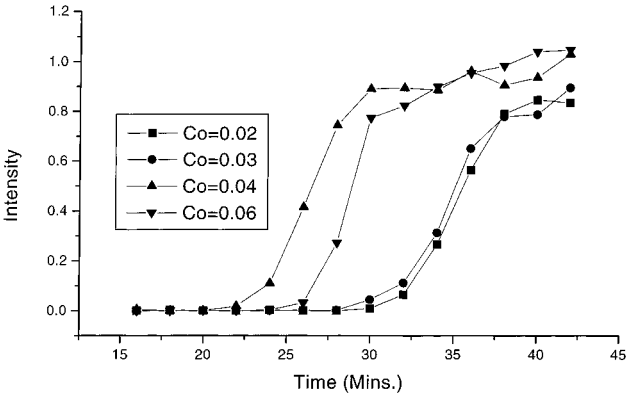

Figure 10. Plots of the normalized area under the reflection which appears at 41 keV (see Figure 8) as a function of time. The different curves represent the measurements carried out at 436 K for various levels of cobalt concentration in the gel under isothermal conditions. (Note that the lines between the points have been added for the sake of clarity and do not represent a mathematical fit.)

Such silicon island formation has been noted in many microporous systems.[32,33] Further investigations are in progress in order to achieve a more detailed explanation of this observation.

Conclusions

Our study has shown that synchrotron-based, time-resolved EDXRD constitutes a powerful technique with which to study crystal growth in microporous materials under realistic in situ hydrothermal conditions. The high levels of time resolution and data quality that can be achieved allow us to follow the structural changes occurring within the system in real time. Coupling EDXRD with other in situ techniques such as combined QuEXAFS/XRD and combined SAXS/WAXS, in addition to more conventional techniques, may lead us toward a much greater understanding of the complete growth process from induction to the end of crystallization. The present study has demonstrated the adequacy of the Avrami−Erofeev model for the kinetics of crystal growth during the hydrothermal synthesis of the zeolite structure**.** Although the results are similar to the those reported from ex situ studies, the present in situ methodolgy provides a unique opportunity to investigate the formation and stability of intermediate phases. The value of the measured activation energy strongly suggests that the activated process relates to the condensation reaction involving formation of Si−O−Si bridges. Framework-incorporated transition-metal ions clearly influence the rate of crystal growth.

Future work will further explore the zeolite A system with regard to other factors that appear to have a profound influence on the kinetics of crystallization such as the type of silica source and the water content of the reaction gel. In addition, these studies will be extended to other, more complex microporous systems with special consideration of the growth and subsequent dissolution of metastable intermediate crystalline phases as well as monitoring competitive formation.

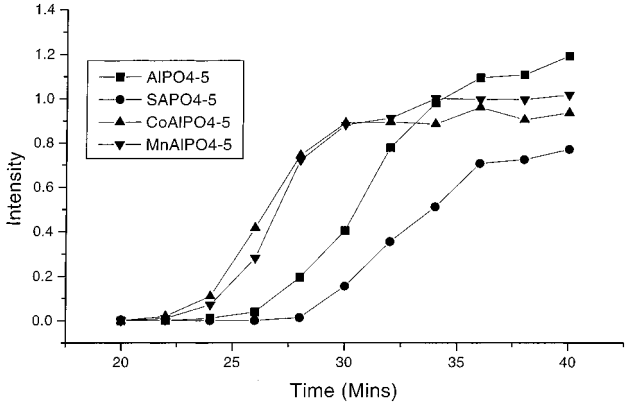

Figure 11. Comparison of the normalized area under the reflection which appears at 41 keV (see Figure 8) as a function of time for $AlPO_4$-5 and for gels containing various heteroatoms (the heteroatom-to-phsophorus ratio in this case being 0.04). The measurements were carried out at 436 K under isothermal conditions. (Note that the lines between the points have been added for the sake of clarity and do not represent a mathematical fit.)

Acknowledgment. We are grateful to EPSRC for supporting this work. We also acknowledge Dr. D. O'Hare for the kind loan of the in situ hydrothermal cell used in these experiments and Dr. F. Rey for useful discussions and comments. Yr ydym yn ddiolchgar am gyfraniad Athro Syr John Meurig Thomas i'r gwaith yma ac i amryw o weithiau eraill ym maes defnyddiau microfandyllog. [English translation: We are grateful for the contribution of Professor Sir John Meurig Thomas to this and many other works in the field of microporous materials.]

References and Notes

(1) Thomas, J. M. *Angew. Chem., Int. Ed. Engl.* **1988,** *27*, 1673−1691.
(2) Davis, M. E. *Acc. Chem. Res.* **1993**, *26*, 111−115.
(3) Davis, M. E.; Lobo, R. F. *Chem. Mater.* **1992,** *4*, 756−768.
(4) Thomas, J. M.; Greaves, G. N.; Catlow, C. R. A. *Nucl. Instrum. Methods Phys. Res. B* **1995,** *97*, 1−10.
(5) Lechert, H. *Zeolites* **1996,** *17*, 473−482.
(6) Weyda, H.; Lechert, H. *Zeolites* **1990**, *10*, 251−258.
(7) Shi, J. M.; Anderson, M. W.; Carr, S. W. *Chem. Mater.* **1996,** *8*, 369−375.

(8) Shigamoto, N.; Sugiyama, S.; Hayashi, H.; Miyaura, K. J. *Mater. Sci. Lett.* **1994,** *13*, 660−662.

(9) Gora, L.; Streletzky, K.; Thompson, R. W.; Phillies, G. D. J. *Zeolites* **1997**, *18*, 119−131.

(10) Twomey, T. A. M.; Mackay, M.; Kuipers, H. P. C. E.; Thompson, R. W. *Zeolites* **1994**, *14*, 162−168.

(11) Schoeman, B. J. *Zeolites* **1997**, *18*, 97−105.

(12) deMoor, P. P. E. A.; Beelen, T. P. M.; Vansanten, R. A. *Microporous Mater.* **1997**, *9*, 117−130.

(13) Dokter, W. H.; Beelen, T. P. M.; Vangarderen, H. F.; Vansanten, R. A.; Bras, W.; Derbyshire, G. E. *J. Appl. Crystallogr.* **1994**, *27*, 901−906.

(14) Dougherty, J.; Iton, L. E.; White, J. W. *Zeolites* **1995**, *15*, 640−649.

(15) Iton, L. E.; Trouw, F.; Brun, T. O.; Epperson, J. E.; White, J. W.; Henderson, S. J. *Langmuir* **1992,** *8*, 1045−1048.

(16) Evans, J. S. O.; Francis, R. J.; O'Hare, D.; Price, S. J.; Clark, S. M.; Flaherty, J.; Gordon, J.; Neild, A.; Tang, C. C. *Rev. Sci. Instrum.***1995,** *66*, 2442−2445.

(17) Gualtieri, A.; Norby, P.; Artioli, G.; Hanson, J. *Microporous Mater.* **1997,** *9*, 189−201.

(18) Munn, J.; Barnes, P.; Häusermann, D.; Axon, S. A.; Klinowski, J. *Phase Transitions* **1992**, *39*, 129−134.

(19) Morris, R. E.; Weigel, S. J.; Norby, P.; Hanson, J. C.; Cheetham, A. K. *J. Synchrotron Radiat.* **1996**, *3*, 301−304.

(20) Norby, P.; Christensen, A. N.; Hansen, J. C. *Stud. Surf. Sci. Catal.* **1994**, *84*, 179−186.

(21) Rey, F.; Sankar, G.; Thomas, J. M.; Barrett, P. A.; Lewis, D. W.; Catlow, C. R. A. *Chem. Mater.* **1995**, *7*, 1435−1436.

(22) Wilson, S. T.; Flanigen, E. M. *ACS Symp. Ser.* **1989,** *398*, 329.

(23) Sankar, G.; Thomas, J. M.; Rey, F.; Greaves, G. N. *J. Chem. Soc., Chem. Commun.* **1995**, 2549−2550.

(24) Raghavan, V.; Cohen, M. *Solid State Phase Transformations. Treatise on Solid State Chemistry;* Hannay, N. B., Ed.; Plenum Press: New York, 1975; Vol. 5, Chapter 2, pp 92−101.

(25) Thompson, R. W. *Zeolites* **1992,** *12*, 680−684.

(26) Budd, P. M.; Myatt, G. J.; Price, C.; Carr, S. W. *Zeolites* **1994,** *14*, 198−202.

(27) Gualtieri, A.; Norby, P.; Artioli, G.; Hanson, J. *Phys. Chem. Miner.* **1997,** *24*, 191−199.

(28) Garfolani, S. H.; Martin, G. *J. Phys. C: Solid State Phys.* **1994**, *98*, 1311.

(29) Pereira, C. Ph.D. Thesis, University of London, 1997.

(30) Lewis, D. W.; Catlow, C. R. A.; Thomas, J. M. *Chem. Mater.* **1996,** *8*, 1112−1118.

(31) Uytterhoeven, M. G.; Schoonheydt, R. A *Proc. 9th Int. Zeolite Conf.* **1992**, 329−336.

(32) Sastre, G.; Lewis, D. W.; Catlow, C. R. A. *J. Phys. Chem.* **1996,** *100*, 6722−6730.

(33) Sastre, G.; Lewis, D. W.; Catlow, C. R. A. *J. Mol. Catal.* **1997,** *119*, 349−356.